Atomic Spectroscopy

Article

A Controllable Spatial Confinement Strategy for Modulating Laser-induced Plasma by Using Inclined Plates

Boping Xu, [a] Junyi Liu, [a] Mengbo Cheng, [a] Lianzhan Wang, [a] Jingyan Wang, [a] Jiajia Hou, [a] Xukun Yin, [a] Jie Tang, [b,*] and Dacheng Zhang [a,*]

[a] School of Optoelectronic Engineering, Xidian University, Xi'an 710071, P. R. China

[b] State Key Laboratory of Ultrafast Optical Science and Technology, Xi'an Institute of Optics and Precision Mechanics of CAS, Xi'an 710119, P. R. China

Received: *July 15, 2026;* ***Revised:*** *September 28, 2026;* ***Accepted:*** *September 28, 2026;* ***Available online:*** *September 30, 2026.*

DOI: 10.46770/AS.2026.0057s

ABSTRACT: Spatial confinement is a simple, efficient, and low-cost modulation strategy for enhancing both the signal intensity and shot-to-shot stability of laser-induced plasmas. However, achieving optimal confinement still relies on repeated experiments because existing shockwave models do not account for cavity configurations. In this work, an inclined plate confinement cavity is developed for the spatial modulation of laser-induced plasmas. The confinement effects of cavities with two typical configurations on plumes are compared and analyzed. The spectral intensities are enhanced and the shot-to-shot spectral fluctuation is reduced by using an inclined plate with an obtuse-angle configuration. The mechanism behind the disparity is demonstrated by shadowgraphs of shockwaves. A theoretical formula for the shockwave is developed by incorporating the cavity characteristic parameters into the model. The developed formula enables accurate prediction of the delay time for the reflected shockwave to propagate back to the plasma generation region in inclined plates. The predicted temporal window agrees well with time-resolved spectroscopic measurements, with a mean absolute error of 0.56 μs. Quantitative analysis of the trace element Mg is also conducted using spatially confined LIBS with inclined plates. The limit of detection of Mg is reduced to one-seventh of that with no cavity by using the inclined plate with an obtuse-angle configuration. This work provides a feasible route for controllable plasma modulation and the synergistic enhancement of plasma signal intensity and stability, facilitating precise quantitative analysis by LIBS.

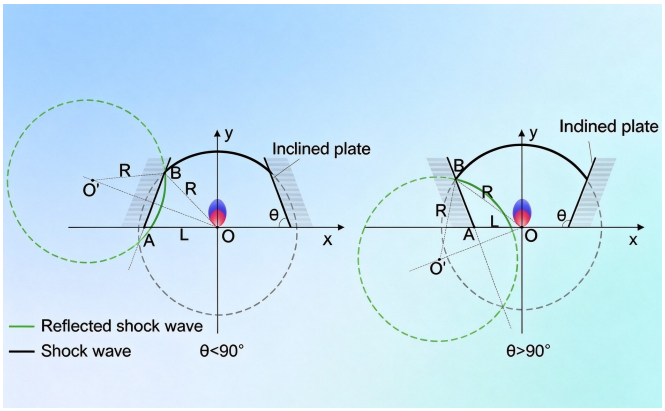

INTRODUCTION

Laser-induced breakdown spectroscopy (LIBS) is a powerful tool with multiple advantages, including simultaneous multi-element analysis, nearly nondestructive analysis, rapid detection, on-line monitoring, and so on, which makes this technology widely regarded as a "future superstar" in chemical analysis.[1] However, its further widespread application is severely hindered by challenges in precise quantitative analysis, primarily due to relatively low signal repeatability and matrix effects. Wang et al. attributed these limitations primarily to the drastic spatiotemporal variations in the laser-induced plasma.[2] The key issues are how to obtain plasma spectra with high signal-to-noise ratios and reproducibility within the spatiotemporal acquisition window of shot-to-shot plasma plumes. For the former issue, researchers proposed various plasma enhancement strategies to increase spectral intensities, such as double-pulse LIBS (DP-LIBS),[3] discharge-assisted LIBS (DA-LIBS),[4] microwave-assisted LIBS (MA-LIBS),[5] nanoparticle surface enhanced LIBS,[6] and so on, where spectral enhancements of more than one order of magnitude are achieved. However, the latter issue of shot-to-shot repeatability remains far from satisfactory, and the signal uncertainty is still a major concern.

Therefore, more efforts should focus on plasma modulation rather than simple signal enhancement in order to improve the stability and repeatability of plasma plumes.[7] Spatial confinement modulation of plasmas is considered an effective, low-cost, and simple strategy for improving the signal intensity and shot-to-shot stability of plasma plumes.[8,9] It was reported that a cylindrical cavity with a moderate size effectively suppresses plasma position fluctuations and stabilizes the plasma radiation, where the relative standard deviation (RSD) for the C I 193 nm line was reduced by 21%, and the spectral intensity was increased by a modest factor of 2.[10] When a geometric confinement structure is placed around the plumes in spatially confined LIBS, the shockwave can be reflected at the boundary and feedback part of its momentum and pressure to the plume, thereby producing a compression effect. Fast imaging and shadowgraphy have revealed that the reflected shockwaves compress the plasma plume into a denser and brighter core.[8,11] Correspondingly, confined plasma plumes exhibit higher plasma temperatures and electron densities than those under unconfined conditions.[12,13] Therefore, plasma modulation in spatially confined LIBS is widely believed to originate from the compression of the plasma plume by reflected shockwaves.[8,12,14]

In essence, the geometric configuration of confinement cavities dictates the reflection paths, delay times, and compression strength of the reflected shockwave.[15] Thus, to optimize the modulation effect on plumes, researchers explored confinement cavities with various geometric configurations, including parallel plates, cylindrical cavities, hemispherical cavities, and rectangular cavities.[13,16,17] Wang et al. experimentally and computationally investigated the expansion dynamics of shockwaves in both flat-surface and parallel plates cases based on Taylor-Sedov theory.[18] The simulation results exhibited good agreement with the experimental results.[19] However, the model established by Wang is restricted to conventional cavity geometries with walls perpendicular to the sample surface and cannot be readily extended to inclined plates configurations with various inclination angles. In our previous study, a conical cavity confinement cavity was proposed.[20] The confinement and modulation effects on the plasma were investigated for two configurations in which the cavity inner walls formed either an obtuse angle or an acute angle with the sample surface. A significant enhancement effect was observed in the cavity with an obtuse-angle configuration. However, the mechanism underlying this disparity is still not fully understood. Unfortunately, the Taylor-Sedov theory does not explicitly incorporate cavity characteristic parameters.[18] Thus, the relationship between shockwave dynamics and cavity characteristic parameters, such as cavity diameter and inner-wall angle, cannot be quantitatively established, thereby limiting its applicability to cavity design and optimal confinement.

To fill this gap, the interaction between the reflected shockwave and plasma plumes in the inclined plate cavity is investigated. Here, time-integrated and time-resolved spectra are studied under different confinement configurations. Shadowgraphs is employed to examine the propagation of shockwaves, thereby demonstrating the mechanism responsible for the observed spectral disparities. Furthermore, a theoretical formula applicable to inclined plates with various configurations is developed by incorporating cavity characteristic parameters into the shockwave model. This formula enables accurate prediction of the delay time for the reflected shockwave to propagate back to the plasma generation region in inclined plates with different configurations. The predicted temporal windows agree well with the time-resolved spectroscopic measurements, with a mean absolute error of 0.56 μs. Quantitative analysis of trace elements in aluminum alloys is also conducted to verify the improvement in analytical precision achieved by using inclined plates with appropriate configurations. As a result, these findings establish a quantitative relationship between shockwave dynamics and cavity characteristic parameters, providing a feasible route for controllable plasma modulation and the synergistic enhancement of plasma signal intensity and stability, thereby facilitating precise quantitative analysis in LIBS.

EXPERIMENTAL

A schematic diagram of the experimental setup for spatially confined LIBS using inclined plates is shown in Fig. 1(a). Here, an excitation laser source (Laser 1) for producing plasmas was a 1064 nm Q-switched Nd:YAG laser (Beamtech, Dawa 300) with a repetition rate of 10 Hz, a pulse duration of 7 ns, and a pulse energy of 50 mJ. The laser beam was reflected by a beam splitter (R:T=1:9), and an energy meter was used to measure 10% of the total laser energy. The ablation laser was focused by a lens (Lens 1) with a focal length of 150 mm onto the aluminum alloy sample surface to induce plasma plumes. The diameter of the ablation spot was about 200 μm. Emission spectra emitted from the laser-induced plasma were reflected by a dichroic mirror (Thorlabs, DMLP805L) and then focused into an optical fiber by a UV-grade quartz lens (Lens 2) with a focal length of 50 mm. The optical fiber with a core diameter of 100 μm was coupled into a spectrometer (Andor Tech., Shamrock 303i) equipped with an intensified CCD camera (Andor Tech., iStar 340t). The spectral range was set as required, and a grating of 600 lines/mm was used to achieve a spectral resolution of 0.1 nm. Another Nd:YAG laser source (Laser 2) served as an irradiation laser to study the dynamics of shockwaves by shadowgraphy. The wavelength, pulse duration, and repetition rate were 532 nm, 7 ns, and 10 Hz, respectively. The probe beam sequentially passed through a half-wave plate and a polarizing beam splitter (PBS). After being expanded by beam-expanding lenses, it traversed the laser-induced plasma and the accompanying shockwave. The shadowgraphs were recorded by a CCD camera (Daheng Imaging, Mer-132-43U3C) equipped with a narrowband optical filter centered at 532 nm, which was

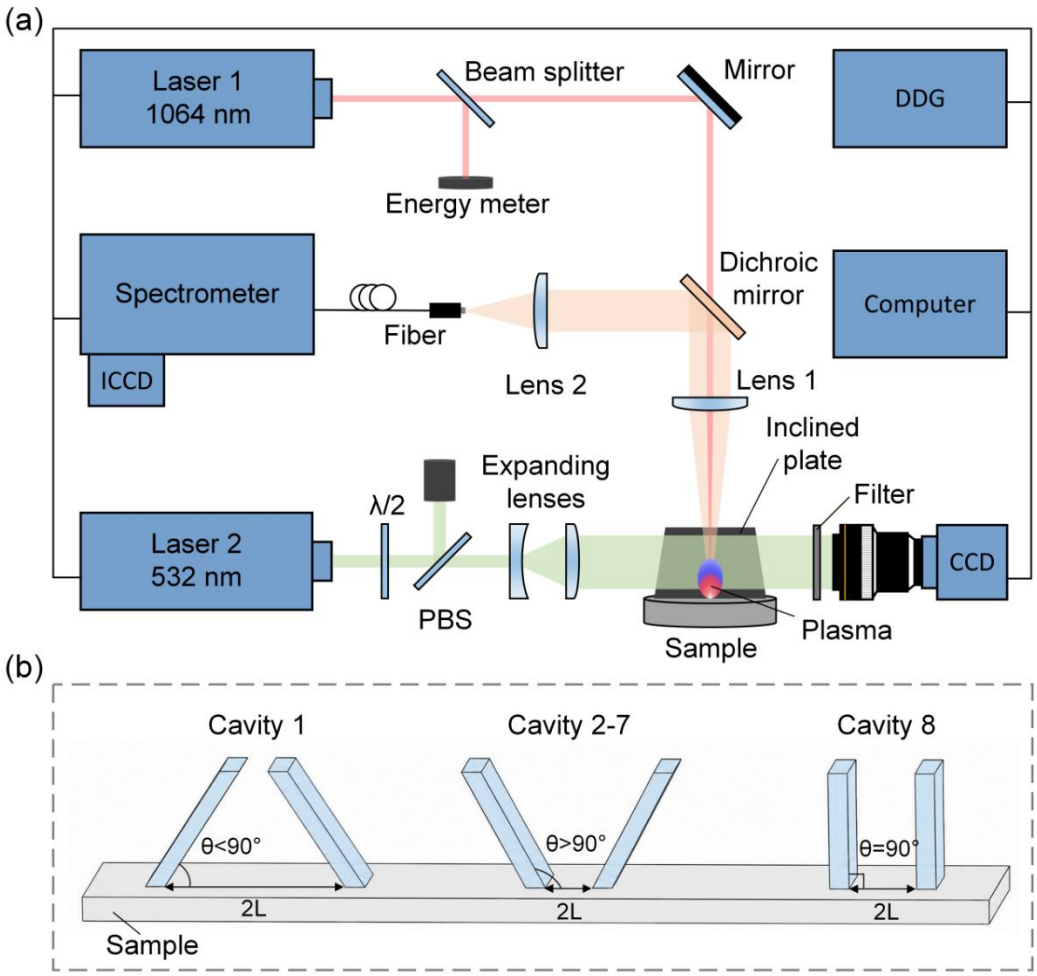

Fig. 1 (a) Schematic diagram of the experimental setup for spatially confined LIBS and shadowgraphy. (b) Schematic of the plate cavities with three configurations. The characteristic parameters of Cavity 1-8 are listed in Table 1.

Table 1. The confinement configurations with different characteristic parameters of θ and 2L

Cavity	**1**	**2**	**3**	**4**	**5**	**6**	**7**	**8**
θ (deg)	65	115	112	108	104	99	94	90
2L (mm)	10	5	2	3	4	5	6	7

mounted in front of the camera lens. The CCD exposure time was fixed at the minimum gate time of 20.00 μs. A digital delay generator (DDG) was employed to synchronize and control the trigger timings of Laser 1, Laser 2, the CCD camera, and the ICCD camera. Shockwaves at different delay times were recorded by adjusting the delay between Laser 1 and Laser 2.

The spatial confinement cavity consisted of a pair of inclined plates symmetrically positioned on both sides of the plasma, with the probe beam passing through the plasma. The geometry of the confinement plates is characterized by two parameters, as shown in Fig. 1(b). One is the angle between the plates and the sample surface, denoted by θ. The other is the distance from the ablation spot to the lower edge of an inclined plate, denoted by L. The characteristic parameters of the various confinement cavities are listed in Table 1. In Cavity 1, the plates form an acute angle with the sample surface, corresponding to an upper aperture that is smaller than the lower aperture. In Cavities 2-7, the plates form an obtuse angle with the sample surface, where the upper aperture is larger than the lower aperture. Cavity 8 represents the special confinement configuration of parallel plates, in which the upper and lower apertures are identical.

The aluminum alloy samples used in this work are certified standard samples (GSB-04-3069-2013) purchased from Southwest Aluminum Co., Ltd. Six standard samples are used for the quantitative analysis, with the mass percentage concentrations of Mg of 1.17%, 0.648%, 0.914%, 0.411%, 0.048%, and 1.52%.

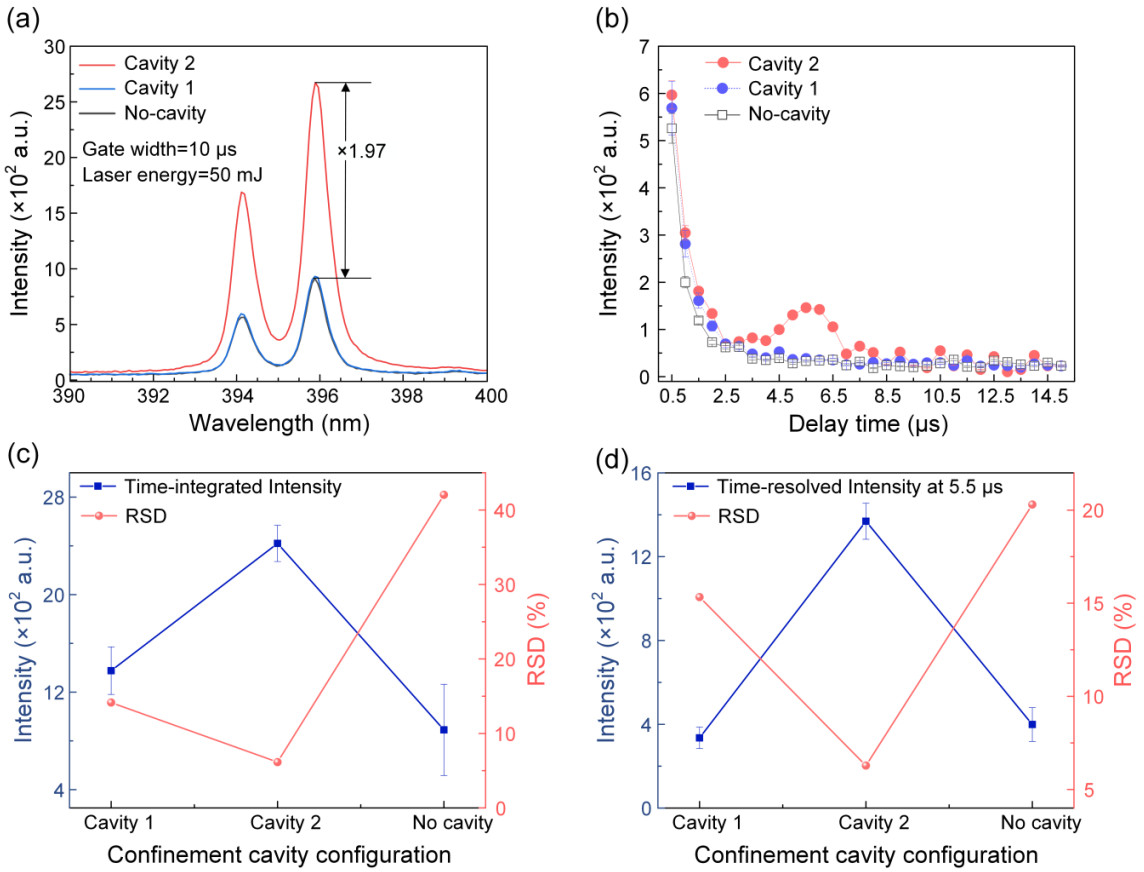

Fig. 2 Spectral characteristics of laser-induced Al plasma. (a) Time-integrated spectra and (b) time-resolved spectral intensities of Al I from the plasma confined in Cavity 1, Cavity 2, and no cavity. (c) Average intensity, standard deviation, and relative standard deviation of Al I from the time-integrated spectra. (d) Corresponding results from the time-resolved spectra.

RESULTS AND DISCUSSION

The spectra and characteristics of Al I from the laser-induced plasma confined in various cases are depicted in Fig. 2. Fig. 2(a) shows the time-integrated spectra from the plasma confined in Cavity 1 and Cavity 2, as well as the plasma without a cavity, where the gate width and gate delay were set at 10.00 μs and 0.50 μs, respectively. It follows from Fig. 2(a) that the time-integrated spectra from the plasma confined in Cavity 2 exhibit an obvious enhancement effect, compared with the case with no cavity. The enhancement factor of Al I 396.1 nm line is 1.97 by using Cavity 2. However, no enhancement effect is observed with Cavity 1.

The time-resolved spectral intensities of Al I 396.1 nm for the plasma confined under various conditions are shown in Fig. 2(b). Here, the gate width and gate step of the ICCD were fixed at 0.50 μs. Error bars represent the standard deviation of spectral intensities obtained from 10 repeated measurements. It is found that the spectral intensities under the three confinement conditions are rapidly reduced from 0.50 μs to 4.00 μs. Then, the spectral intensity for Al I from the plasma in Cavity 2 begins to increase, compared with the case without a cavity. The most significant enhancement effect is observed at 5.50 μs, and this enhancement effect lasts until about 8.50 μs. In contrast, there is no enhancement effect on spectral intensity when Cavity 1 is present. The emission intensity monotonously declines as same as the time-resolved spectra with no cavity confinement. These findings are consistent with our previous studies on the laser-induced copper plasma.[20,21]

It is well known that the spectral enhancement induced by spatial confinement originates from the compression and modulation of the plasma by the reflected shockwaves. As the shockwave propagates outward and encounters the confinement boundaries, it is reflected toward the plasma. The reflected shockwave subsequently interacts with and compresses the plasma plume, suppressing its expansion and increasing the collision probability among the plasma species.[12,13] As a result, the population density of highly excited particles is increased, leading to enhanced optical emission.[22] In our previous study,[20] the plasma temperature and electron number density of the plumes confined in two typical conical cavities were systematically investigated. When the inner

wall inclination angle is obtuse (similar to that of Cavity 2), the plasma exhibits a higher temperature and electron density. This provides direct evidence for the increased spectral intensity.

In order to investigate the effect of spatial confinement with inclined plates on the plasma stability, the average spectral intensity, standard deviation (SD), and relative standard deviation (RSD) of Al I 396.1 nm from the shot-to-shot plasma in Cavity 1, Cavity 2, and without a cavity are determined. The results of time-integrated spectral intensities are shown in Fig. 2(c). Here, the gate width was 10 μs, and the error bars represent the SD of 10 measurements. It can be seen that the spectral intensity in Cavity 1 is comparable to that without a cavity. Meanwhile, the SD decreases from 374 to 194, and the RSD decreases from 42.1% to 14.1%. For Cavity 2, the spectral intensity increases significantly, reaching 1.7 times the value obtained without a cavity. More importantly, the SD decreases to 148, and the RSD is further reduced to 6.1%.

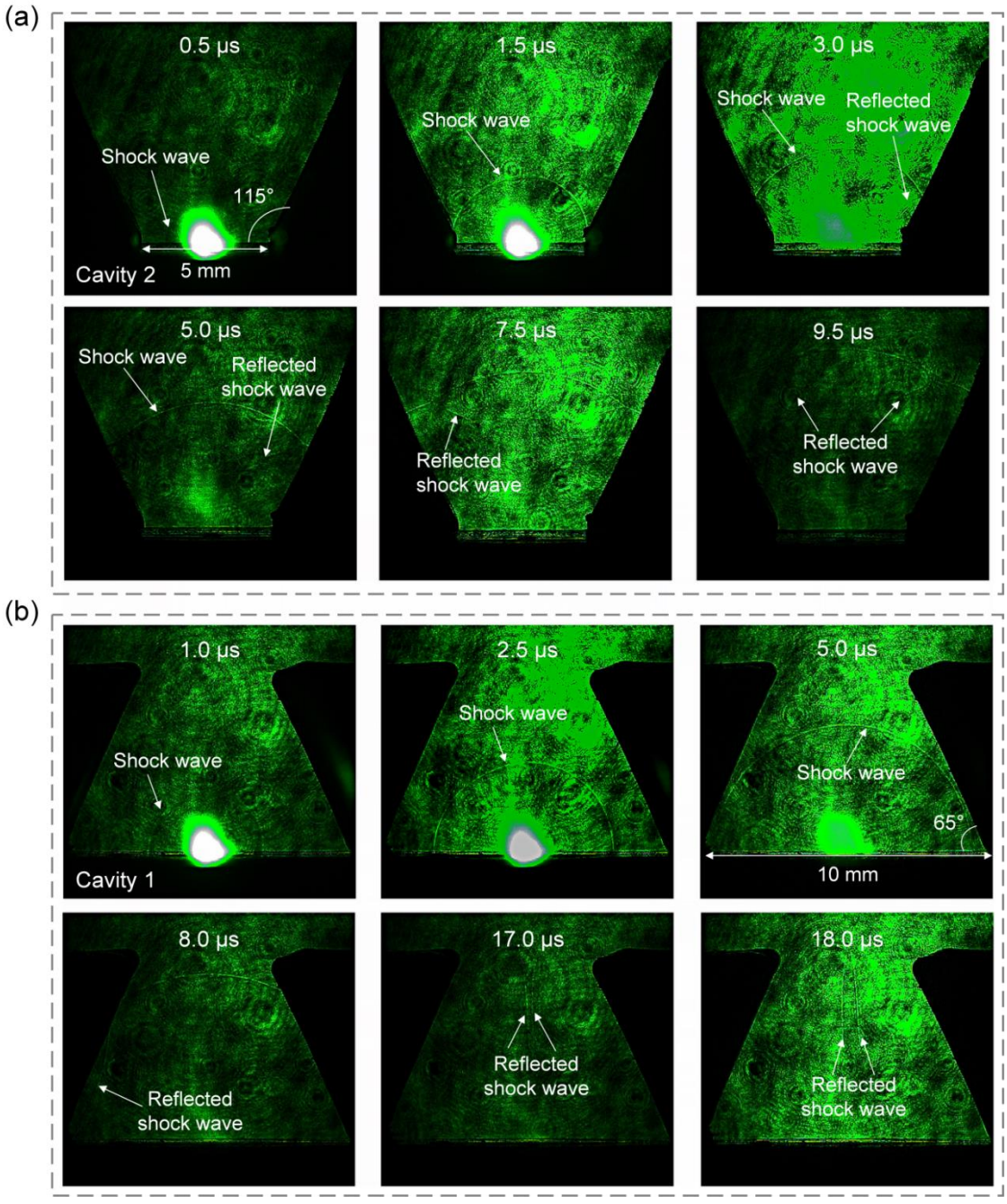

Fig. 3 Shadowgraphs of shockwave from Al plasma confined in (a) Cavity 2 and (b) Cavity 1.

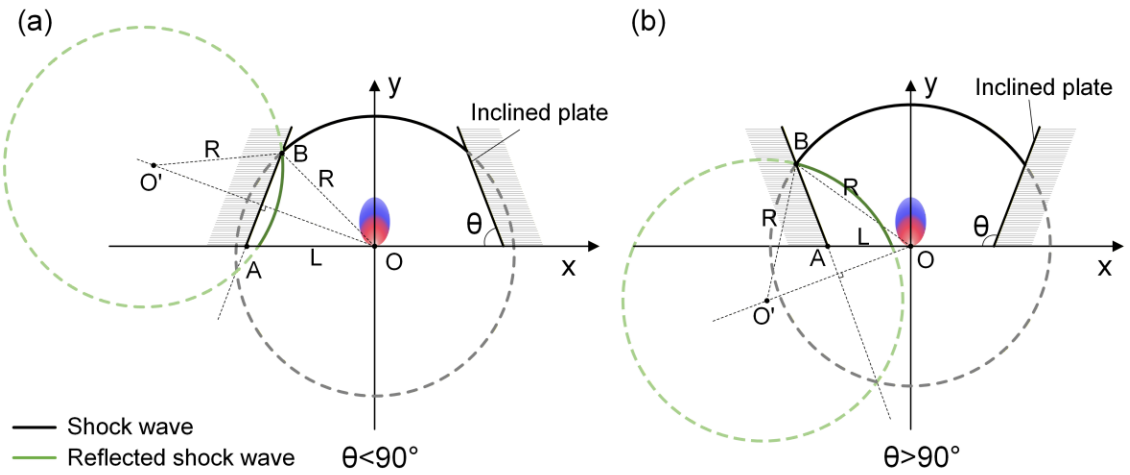

Fig. 4 Theoretical model of shockwave in the inclined plate cavities (a) with an acute angle θ and (b) with an obtuse angle θ.

Figure 2(d) presents the average time-resolved spectral intensity, SD, and RSD of the Al I 396.1 nm line at a delay time of 5.5 μs, at which the maximum spectral enhancement is achieved. Similar to the time-integrated results without confinement the spectral intensity and SD are the lowest, while the RSD reaches 20.3%. With Cavity 1, the RSD decreases to 15.3%. With Cavity 2, the spectral intensity increases to 2.4 times that without a cavity. More importantly, the RSD is further reduced to 6.3% due to the spatial confinement modulation. It should be noted that the improvement of RSD achieved with spatial confinement in LIBS is attributable to the enhanced stability of plasma morphology brought by the modulation of reflected shockwaves, rather than the increase in spectral signal intensity.

To further investigate the disparities in spectral enhancement behavior, shadowgraphy was employed to study the interaction between the shockwave and the plasma. The shadowgraphs obtained in Cavity 2 and Cavity 1 at various delay times are shown in Figs. 3(a) and 3(b), respectively. As shown in Fig. 3(a), a distinct hemispherical shockwave structure is observed at a delay time of 0.50 μs in Cavity 2. When the delay time increases to 1.50 μs, the shockwave reaches the inner surface of the inclined plates. Reflected shockwaves become visible after approximately 3.00 μs. At a delay time of 5.00 μs, it is observed that the reflected shockwaves arrive at the plasma region and interact with the plasma plume. This observation is consistent with the time-resolved spectra, where Cavity 2 yields the maximum enhancement effect at 5.50 μs as shown in Fig. 2(b). This interaction effectively compresses and modulates the plasma and is considered the primary mechanism responsible for the observed spectral enhancement. At later delay times of 7.50 μs and 9.50 μs, the reflected shockwave continues to propagate and expand outward. As the plasma dissipates, the reflected shockwave can no longer compress the plasma plume again. Thus, no spectral enhancement is observed at later time.

In comparison, it follows from Fig. 3(b) that clear hemispherical shockwaves are also observed at 1.00 μs and 2.50 μs in Cavity 1. However, unlike Cavity 2, the shockwave is still propagating outward at 5.00 μs. This time corresponds to the time window in which significant spectral enhancement is observed in Cavity 2. At this moment, the shockwave has not yet reached the inner surface of the inclined plates and therefore cannot generate reflected shockwaves capable of modulating the plasma. Reflected shockwaves are first observed at approximately 8.00 μs. They reach the vicinity of the plasma at about 17.00 μs.

By combining the shadowgraphs with the time-resolved spectral results, the disparity in confinement enhancement between Cavity 2 and Cavity 1 can be clearly understood. The time-resolved spectral intensity demonstrates that the lifetime of plasma plumes is about 8.00 μs. Previous fast imaging studies demonstrated that plasma plumes under atmospheric conditions generally exhibit characteristic dimensions of approximately 3–5 mm in length and 1–2 mm in width.[23] In Cavity 2, the reflected shockwaves reach the plasma center at approximately 5.00 μs, when the plasma still contains abundant emitting species. The reflected shockwave with sufficient energy compresses the plume, thereby increasing the density of emitting species and leading to pronounced spectral enhancement. In contrast, the reflected shockwaves in Cavity 1 reach the vicinity of the plasma at about 17.00 μs, as observed in Fig. 3(b). At this moment, the plasma largely decays, while the reflected shockwaves also experience substantial energy dissipation during propagation. Consequently, the interaction between the shockwaves and the plasma becomes too weak to produce effective compression, which explains the absence of observable spectral enhancement in the plasma spectra.

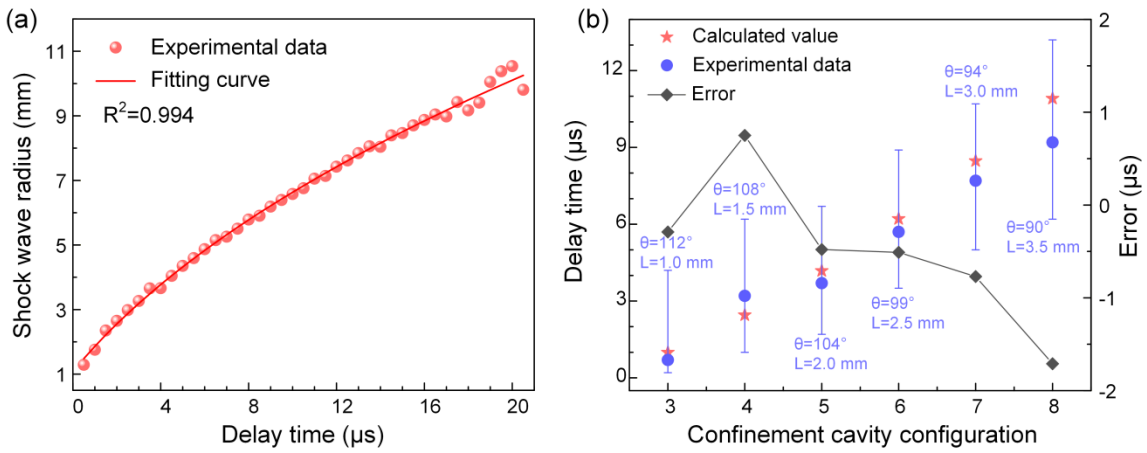

Fig. 5 (a) Radius of the expanding shockwave as a function of delay time. (b) Theoretical and experimental delay time of the interaction between reflected shockwave and plasma plume confined in various cavity configurations. Errors are referred to as the differences between the theoretical and experimental values.

To further investigate the propagation behavior of shockwaves from plasmas confined in the inclined plate cavities, a shockwave reflection model was developed based on shockwave theory.[18] The schematic diagrams of the theoretical model for inclined plates with acute and obtuse angles are shown in Figs. 4(a) and 4(b), respectively. For simplicity, the shockwave is assumed to expand as an ideal spherical wave, and its interaction with the cavity walls is treated as a perfectly elastic reflection. In Fig. 4, point O represents the ablation spot, and the distance between point O and the lower edge of an inclined plate (point A) is denoted by L. The angle between the plate and the sample surface is denoted by θ. Point B corresponds to the location where the shockwave first contacts the inner wall of the plate. Therefore, OB is equal to the radius R of the shockwave. Upon reaching the cavity wall, the shockwave is reflected symmetrically with respect to line AB.[24] According to the geometric relationship, the center of the reflected spherical shockwave, denoted by point O', is located at:

$$(-2L\sin^2\theta,\ 2L\sin\theta\cos\theta). \tag{1}$$

The position of point O' is uniquely determined by the parameters L and θ. And O'B is equal to the radius R of the reflected shockwave. When the reflected shockwave propagates back to the origin O, the reflected shockwave radius is equal to the distance O'O, which can be expressed as:

$$O'O=2L\sin\theta. \tag{2}$$

This result indicates that the propagation distance required for the reflected shockwave to return to the ablation spot depends solely on L and θ. Based on this model, a predictive confinement strategy is proposed for controllable modulation of laser-induced plasmas at predetermined times. By considering the Taylor-Sedov theory,[18]

$$R=\left(\frac{E_0}{K(\gamma)\rho_0}\right)^{1/5} t^{2/5}, \tag{3}$$

the reflected shockwave can be controlled to reach the plasma center at any desired time, by regulating the characteristic parameters of L and θ of the inclined plates as shown in the following equation:

$$2L\sin\theta=\left(\frac{E_0}{K(\gamma)\rho_0}\right)^{1/5} t^{2/5}, \tag{4}$$

where E_0 is the ablation energy, $K(\gamma)$ is a constant related to the adiabatic index of the ambient gas, ρ_0 is the density of the undisturbed ambient gas. Therefore, in theory, the specific formula, associated with the Taylor-Sedov theory, is improved to a universal one that is suitable for more application scenes.

In practice, to further validate the proposed spatial confinement modulation strategy for laser-induced plasma, the temporal evolution of the shockwave radius is fitted using Eq. (3), as shown in Fig. 5(a). The fitting results exhibit good agreement with the measurements, with a coefficient of determination (R^2) exceeding 0.99. Based on Eq. (4), the theoretical delay times corresponding to the arrival of the reflected shockwave at the ablation spot are calculated for different cavity configurations, and the results are presented in Fig. 5(b). Meanwhile, time-resolved spectroscopic measurements are conducted in various confinement cavity configurations, in order to determine the onset and termination times of spectral enhancement in different cases. These times are represented as the lower and upper bounds of the bars, respectively. The blue solid circles in Fig. 5(b) represent the delay times corresponding to the maximum spectral enhancement effect.

It can be seen that all theoretical predictions fall within the time intervals during which spectral enhancement is observed.

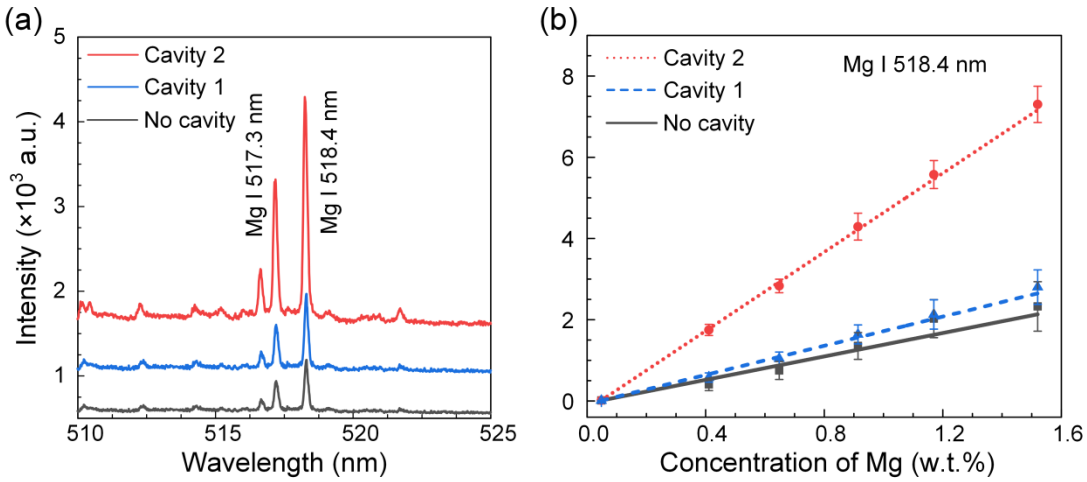

Fig. 6 Quantitative analysis of Mg in the aluminum standard samples using spatial confinement LIBS with Cavity 1, Cavity 2, and no cavity. (a) Time-integrated spectra for Mg I in different confinement cases. (b) Calibration curves for Mg I 518.4 nm in different confinement cases.

Table 2. Results of the quantitative analysis of Mg in different confinement cases

Element	Cavity 2			Cavity 1			No cavity		
Mg I 518.4 nm	b	$\sigma_{y/x}$	LOD (wt.%)	b	$\sigma_{y/x}$	LOD (wt.%)	b	$\sigma_{y/x}$	LOD (wt.%)
	4855	75	0.063	1793	140	0.321	1441	156	0.443

Furthermore, the experimental data exhibit the same trend as the theoretical results. The delay time gradually increases with increasing L and decreasing θ. As for the inclined plates, such as Cavities 3-7, the errors between the theoretical and experimental values range from -0.77 μs to 0.75 μs, and the mean absolute error (MAE) is calculated to be only 0.56 μs, close to the gate width of 0.50 μs. Moreover, the predicted delay time for the reflected shockwave to reach the ablation spot in Cavity 1 (θ<90°) is 16.68 μs. This value agrees well with the shadowgraphs in Fig. 3(b), where the reflected shockwave return to plasma at 17.00 μs. In contrast, as for Cavity 8, i.e., the parallel plate, the error is increased to -1.71 μs. In this case, the shockwave compresses the lateral sides of the plasma rather than its bottom surface. Besides, a strong plasma compression and enhancement effect is induced by the shockwave before the shockwave reaches the origin. These phenomena indicate that the model is more suitable for confinement cavities with inclined plates, and is able to predict the delay time at which the maximum spectral enhancement occurs. The above findings validate the effectiveness of the proposed laser-induced plasma modulation strategy.

In order to investigate the effect of spatial confinement with inclined plates on sensitivity of LIBS, the trace element Mg in the aluminum alloy is quantitatively analyzed. Fig. 6 depicts the results of the quantitative analysis of Mg in the alloy. The time-integrated spectra of Mg I in the range of 510–525 nm obtained by spatial confinement LIBS with Cavity 1, Cavity 2, and no cavity are shown in Fig. 6(a). It is clearly seen that Mg I 517.3 nm and 518.4 nm from the plasma confined in Cavity 2 exhibit stronger emission, compared to the cases with Cavity 1 and no cavity. Fig. 6(b) depicts the calibration curves for Mg I 518.4 nm in various cases. The limit of detection (LOD) is calculated using the new IUPAC formula proposed by Palleschi *et al.*,[25] which is expressed as follows.

$$\mathrm{LOD} = \frac{3.3\sigma_{y/x}\sqrt{1+\dfrac{\bar{C}^2}{\sum(C_i-\bar{C})^2}}}{b}, \tag{5}$$

where:

$$\sigma_{y/x} = \sum\frac{\sqrt{(I_i-\hat{I}_i)^2}}{N} \tag{6}$$

where N represents the number of points in the calibration curve. The term $\sigma_{y/x}$ is an estimate of the deviation of the signals I_i with respect to the value predicted by the calibration curve $\hat{I}_i$ at that concentration. C_i are the concentrations of the standards and $\bar{C}$ is the average of these concentrations. The term represents the leverage of the blank sample. The higher the leverage, the higher would be the fluctuations of the intercept of the calibration curve, which reflects the uncertainty of the signals.

According to Eq. (5), the LODs for Mg under the three different conditions are calculated, and the results are listed in Table 2. The experimental results show that Cavity 2 provides the highest calibration curve slope, which is 3.4 times that obtained without a cavity and 2.7 times that obtained with Cavity 1. This result is consistent with the time-integrated spectra presented previously.

The calculated LOD of Mg using Cavity 2 is 0.063 wt.%, which is approximately one-seventh of that obtained under the unconfined condition (0.443 wt.%). This improvement can be attributed to the increased spectral intensity and reduced $\sigma_{y/x}$ resulting from the improved signal stability. In addition, Cavity 1 also reduces the LOD of Mg to 0.321 wt.%.

CONCLUSION

In this work, the confinement effects of the inclined plates with various configurations on laser-induced plasmas were investigated by optical emission spectroscopy and shadowgraphy. The spectra show that the obtuse-angle inclined plate exhibits superior confinement modulation, achieving stronger spectral intensities and lower RSD, compared to cases with no cavity and with acute-angle inclined plate. Shadowgraphs of the shockwaves demonstrate that this disparity originates from the more effective compression of the plasma plume by reflected shockwaves at appropriate delay times in the obtuse-angle inclined plate. Furthermore, a theoretical formula applicable to inclined plates with various configurations for spatial confinement of laser-induced plasma is developed, by incorporating the critical characteristic parameters of inclined plates into the shockwave theory. In this model, the laser-induced plasma is able to be modulated at predetermined times by regulating the characteristic parameters of inclined plates. By comparing the theoretical and experimental results under five configurations, the theoretical delay times for the reflected shockwave to reach the plasma center exhibit the same trend as the experimental results, with a mean absolute error of 0.56 μs. Quantitative analysis of the trace element Mg is also conducted using spatially confined LIBS with inclined plates. The limit of detection of Mg is reduced to one-seventh of that with no cavity using the inclined plate with an obtuse-angle configuration. These findings establish a quantitative relationship between shockwave dynamics and cavity characteristic parameters, providing a feasible route for controllable plasma modulation and the synergistic enhancement of plasma signal intensity and stability, facilitating LIBS precise quantitative analysis.

AUTHOR INFORMATION

Jie Tang received his Ph.D. degree from the Xi'an Institute of Optics and Precision Mechanics, Chinese Academy of Sciences, in 2011. He is currently a researcher at the State Key Laboratory of Ultrafast Optical Science and Technology of the Xi'an Institute of Optics and Precision Mechanics. His research focuses on the diagnosis and application of laser plasma and atmospheric gas-discharge plasma.

Dacheng Zhang received his Ph.D degree from the Institute of Modern Physics, Chinese Academy of Science, in 2012. He now is a professor of the School of Optoelectronic Engineering, Xidian University. His main research interests are laser spectroscopy and laser technology, including laser plasma spectroscopy technology and applications, laser resonance ionization, tunable laser technology, laser cooling of ions in accelerator, etc. His group have developed several kinds of portable lasers with high peak power for LIBS, tunable laser with ultra-narrow linewidth for isotope analysis and optical parametric oscillator for laser induced fluorescence spectroscopy.

Corresponding author

* J. Tang

Email address: angjie@opt.ac.cn

* D. C. Zhang

Email address: dch.zhang@xidian.edu.cn

Notes

The authors declare no competing financial interest.

ACKNOWLEDGMENTS

This work was supported by the National Natural Science Foundation of China (62605329, U2241288, and 62475204), the China Postdoctoral Science Foundation (2025M770839), and the Natural Science Basic Research Program of Shaanxi Province (2026JC-YBQN-0857 and 2026JC-QYCX-059).

REFERENCES

1. J. D. Winefordner, I. B. Gornushkin, T. Correll, E. Gibb, B. W. Smith, and N. Omenetto, *J. Anal. At. Spectrom.*, 2004, **19**, 1061–1083. https://doi.org/10.1039/B400355C
2. P. Zheng, G. Chen, W. Gu, J. Wang, Z. Hou, X. Gao, A. Chen, W. Zhou, L. Guo, Q. Zeng, and Z. Wang, *TrAC Trends Anal. Chem.*, 2026, **197**, 118709. https://doi.org/10.1016/j.trac.2026.118709
3. M. Cui, Y. Deguchi, Z. Wang, Y. Fujita, R. Liu, F.-J. Shiou, and S. Zhao, *Spectrochim. Acta B*, 2018, **142**, 14–22. https://doi.org/10.1016/j.sab.2018.02.007
4. W. Zhou, K. Li, Q. Shen, Q. Chen, and J. Long, *Opt. Express*, 2010, **18**, 2573–2578. https://doi.org/10.1364/OE.18.002573
5. E. Q. Oreste, A. O. de Souza, C. C. Pereira, D. H. Bonemann, M. A. Vieira, L. de M. Fontes, C. Pasquini, and A. S. Ribeiro, *Microchem. J.*, 2021, **168**, 106452. https://doi.org/10.1016/j.microc.2021.106452

6. Y. Yao, F. He, Q. Lin, Y. Tian, T. Zhang, B. Xu, X. Qi, and Y. Duan, *J. Anal. At. Spectrom.*, 2021, **36**, 2639–2648. https://doi.org/10.1039/D1JA00247A
7. B. Xu, Z. Feng, J. Hou, S. Wang, D. Zhang, and H. Xu, *Ultrafast Sci.*, 2025, **5**, 0114. https://doi.org/10.34133/ultrafastscience.0114
8. Z. Hou, Z. Wang, J. Liu, W. Ni, and Z. Li, *Opt. Express*, 2013, **21**, 15974–15985. https://doi.org/10.1364/OE.21.015974
9. H. Yin, Z. Hou, T. Yuan, Z. Wang, W. Ni, and Z. Li, *J. Anal. At. Spectrom.*, 2015, **30**, 922–928. https://doi.org/10.1039/C4JA00426A
10. Z. Wang, Z. Hou, S. Lui, D. Jiang, J. Liu, and Z. Li, *Opt. Express*, 2012, **20**, A1011–A1020. https://doi.org/10.1064/OE.20.0A1011
11. X. Gao, L. Liu, C. Song, and J. Lin, *J. Phys. D: Appl. Phys.*, 2015, **48**, 175205. https://doi.org/10.1088/0022-3727/48/17/175205
12. X. Zeng, X. Mao, S. S. Mao, S.-B. Wen, R. Greif, and R. E. Russo, *Appl. Phys. Lett.*, 2006, **88**, 061502. https://doi.org/10.1063/1.2172740
13. L. B. Guo, C. M. Li, W. Hu, Y. S. Zhou, B. Y. Zhang, Z. X. Cai, X. Y. Zeng, and Y. F. Lu, *Appl. Phys. Lett.*, 2011, **98**, 131501. https://doi.org/10.1063/1.3570648
14. L. B. Guo, W. Hu, B. Y. Zhang, X. N. He, C. M. Li, Y. S. Zhou, Z. X. Cai, X. Y. Zeng, and Y. F. Lu, *Opt. Express*, 2011, **19**, 14067–14074. https://doi.org/10.1364/OE.19.014067
15. X. Su, W. Zhou, and H. Qian, *Opt. Express*, 2014, **22**, 28437–28445. https://doi.org/10.1364/OE.22.028437
16. Q. Wang, A. Chen, D. Zhang, Y. Wang, L. Sui, S. Li, Y. Jiang, and M. Jin, *Phys. Plasmas*, 2018, **25**, 073301. https://doi.org/10.1063/1.5031340
17. X. K. Shen, J. Sun, H. Ling, and Y. F. Lu, *Appl. Phys. Lett.*, 2007, **91**, 081501. https://doi.org/10.1063/1.2772760
18. G. I. Taylor, *Proc. R. Soc. London, Ser. A*, 1950, **201**, 159–174. https://doi.org/10.1098/rspa.1950.0049
19. Y. Wang, H. Yuan, Y. Fu, and Z. Wang, *Spectrochim. Acta B*, 2016, **126**, 44–52. https://doi.org/10.1016/j.sab.2016.04.004
20. B. Xu, Y. Liu, B. Lei, J. Wang, W. Zhang, Y. Wang, W. Zhao, Y. Duan, and J. Tang, *Spectrochim. Acta B*, 2022, **197**, 106528. https://doi.org/10.1016/j.sab.2022.106528
21. Y. Liu, B. Xu, B. Lei, S. Liu, J. Wang, J. Zeng, Y. Wang, Y. Duan, W. Zhao, and J. Tang, *Appl. Phys. B*, 2022, **128**, 103. https://doi.org/10.1007/s00340-022-07822-4
22. X. K. Shen, J. Sun, H. Ling, and Y. F. Lu, *J. Appl. Phys.*, 2007, **102**, 093301. https://doi.org/10.1063/1.2800252
23. N. Glumac and G. Elliott, *Opt. Lasers Eng.*, 2007, **45**, 27–35. https://doi.org/10.1016/j.optlaseng.2006.04.006
24. X. Li, Z. Wang, X. Mao, and R. E. Russo, *J. Anal. At. Spectrom.*, 2014, **29**, 2127–2135. https://doi.org/10.1039/C4JA00193A
25. F. Poggialini, S. Legnaioli, B. Campanella, B. Cocciaro, G. Lorenzetti, S. Raneri, and V. Palleschi, *Appl. Sci.*, 2023, **13**, 3642. https://doi.org/10.3390/app13063642